Journal of Nuclear Materials 377 (2008) 427–437

Contents lists available at ScienceDirect

Journal of Nuclear Materials

journal homepage: www.elsevier.com/locate/jnucmat

Embrittlement of irradiated ferritic/martensitic steels in the absence of irradiation hardening

R.L. Klueh [a,*], K. Shiba [b], M.A. Sokolov [a]

[a] Oak Ridge National Laboratory, Materials Science and Technology Division, P.O. 2008 MS6138, Oak Ridge, TN 37831-6138, USA
[b] Japan Atomic Energy Agency, Toki-Mura, Ibaraki, Japan

ARTICLE INFO

Article history:
Received 8 January 2008
Accepted 1 April 2008

ABSTRACT

Irradiation damage caused by neutron irradiation below 425–450 °C of 9–12% Cr ferritic/martensitic steels produces microstructural defects that cause an increase in yield stress. This irradiation hardening causes embrittlement observed in a Charpy impact test as an increase in the ductile–brittle transition temperature. Little or no change in strength is observed in steels irradiated above 425–450 °C. Therefore, the general conclusion has been that no embrittlement occurs above these temperatures. In a recent study, significant embrittlement was observed in F82H steel irradiated at 500 °C to 5 and 20 dpa without any change in strength. Earlier studies on several conventional steels also showed embrittlement effects above the irradiation-hardening temperature regime. Indications are that this embrittlement is caused by irradiation-accelerated or irradiation-induced precipitation. Observations of embrittlement in the absence of irradiation hardening that were previously reported in the literature have been examined and analyzed with computational thermodynamics calculations to illuminate and understand the effect.

1. Introduction

Ferritic/martensitic steels are the only viable structural material for first wall and blanket structures of future fusion reactors. In the United States Department of Energy fusion materials program, the first ferritic/martensitic steels considered were commercial Sandvik HT9 and modified 9Cr–1Mo (ASTM Grade 91). Similar commercial steels were considered in European and Japanese fusion programs. These 9–12Cr–MoVNb steels were subsequently replaced by the development of 'reduced-activation' 7–9Cr–WVTa steels. The objective for reduced-activation steels is to replace alloying elements that lead to long-lasting radioactive transmutation products with elements that produce products that decay rapidly. Molybdenum and niobium in commercial Cr–MoWVNb steels were replaced by tungsten and tantalum. The advantage of reduced-activation steels is that nuclear waste for such steels can be more easily disposed.

Neutron-irradiation effects on the mechanical properties of commercial and reduced-activation ferritic/martensitic steels have been studied extensively [1]. High-energy neutron irradiation displaces atoms from their normal positions to form vacancies and interstitials. It is the disposition of the 'displacement damage', measured as displacements per atom (dpa), that affects the mechanical properties. The progressive change in microstructure with irradiation dose and temperature involves the agglomeration of vacancies and interstitials into voids and dislocation loops that lead to swelling and hardening. Irradiation-induced segregation and precipitation also occur.

Agglomeration of vacancies leads to void swelling up to about 500 °C. Dislocation loops cause hardening below about 425–450 °C, with the loop size increasing and loop number density decreasing as irradiation temperature is increased. With increasing temperature, loops evolve into a dislocation structure [2–6]. Above 425–450 °C, more rapid diffusion allows the irradiation-induced defects to anneal out and precipitates to coarsen.

The effect of neutron-irradiation on the tensile behavior of 5–12% Cr ferritic/martensitic steels also depends on temperature [7–10]. Below ≈425 °C, dislocation loop formation causes the steels to harden, which leads to an increased yield stress and ultimate tensile strength (Fig. 1) and decreased ductility (Fig. 2). Hardening saturates with irradiation fluence, as seen in Fig. 3 for the yield stress of HT9 irradiated in the EBR-II (Experimental Breeder Reactor) to ≈13 and 25 dpa at 390–550 °C [8,10]. Yield stress is the same after 13 and 25 dpa at 390 °C [10]. The saturation fluence varies inversely with temperature. At 400 °C, the saturation dose is <10 dpa [8]. When irradiation is above ≈425 °C, tensile properties are generally unchanged (Figs. 1 and 3), although there may be irradiation-enhanced softening, depending on fluence and temperature [8–10].

Irradiation hardening affects other properties, such as fatigue and toughness. The latter is of major concern and has received considerable attention in the development of steels for fusion reactor applications and in studies of the pressure-vessel steels used in

* Corresponding author. Tel.: +1 865 574 5111; fax: +1 865 241 3650.
E-mail address: kluehrl@ornl.gov (R.L. Klueh).

0022-3115/$ - see front matter © 2008 Elsevier B.V. All rights reserved.
doi:10.1016/j.jnucmat.2008.04.002

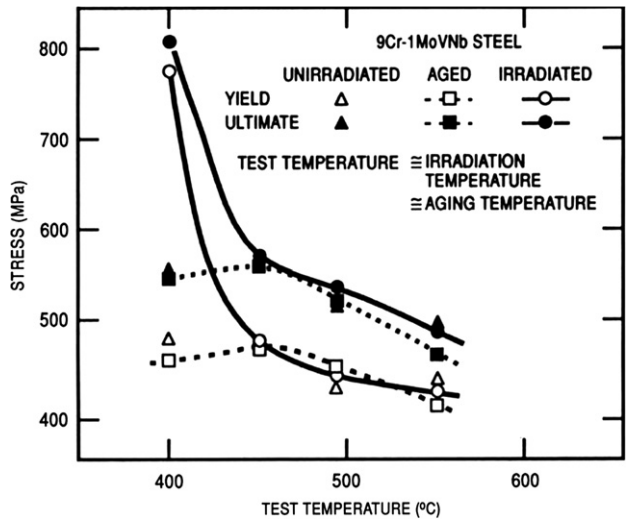

Fig. 1. Yield stress and ultimate tensile strength of modified 9Cr–1Mo (9Cr–1MoVNb) steel in the unirradiated, thermally aged, and irradiated conditions. Irradiation was in EBR-II to ≈12 dpa at 390, 450, 500, and 550 °C; tensile tests and thermal aging were carried out at the irradiation temperatures [8].

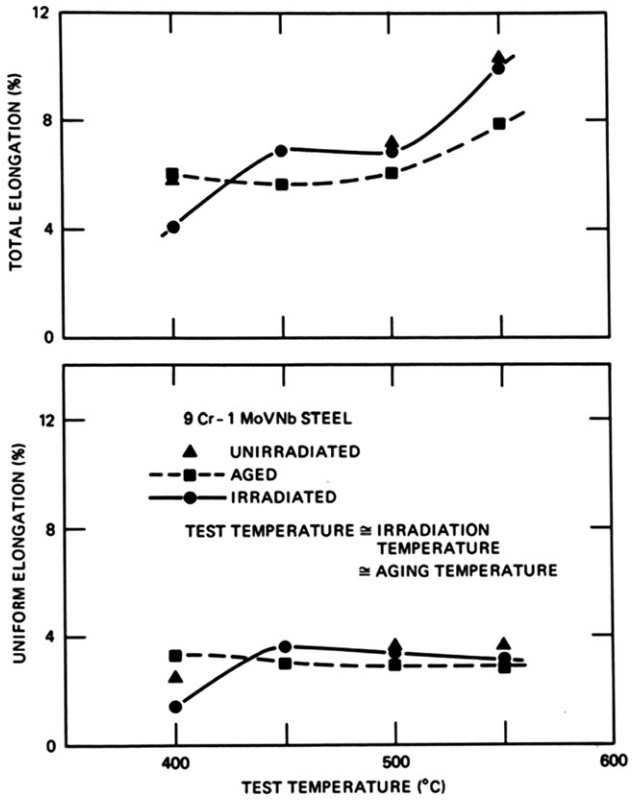

Fig. 2. Uniform and total elongation of modified 9Cr–1Mo (9Cr–1MoVNb) steel in the unirradiated, thermally aged, and irradiated conditions. Irradiation was in EBR-II to ≈12 dpa at 390, 450, 500, and 550 °C; tensile tests and thermal aging were carried out at the irradiation temperatures [8].

light-water reactors. The effect of irradiation hardening on toughness is observed qualitatively in a Charpy impact test as an increase in the ductile–brittle transition temperature (DBTT) and a decrease in upper-shelf energy (USE) [11–16]. For Sandvik HT9 irradiated in the Fast Flux Test Facility (FFTF) at 365 °C (Fig. 4) [11], the increase in DBTT (ΔDBTT) saturates with fluence (the shift is the same after 10 and 17 dpa) in the same way as the yield stress

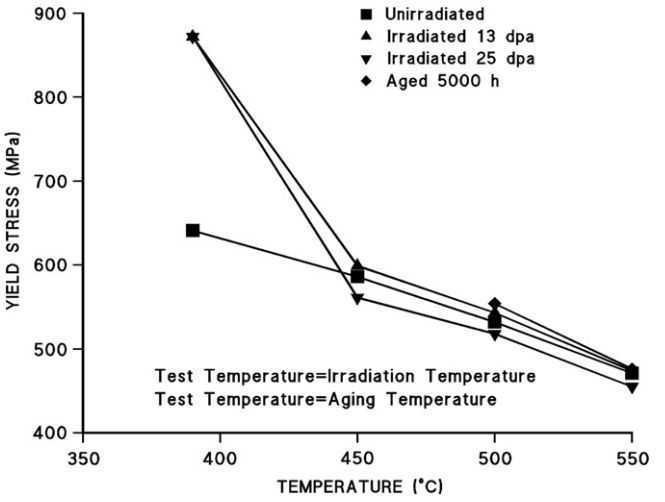

Fig. 3. Yield stress of modified Sandvik HT9 steel in the unirradiated, thermally aged, and irradiated conditions. Irradiation was in EBR-II to ≈13 and 25 dpa at 390, 450, 500, and 550 °C; tensile tests and thermal aging were carried out at the irradiation temperatures [10]

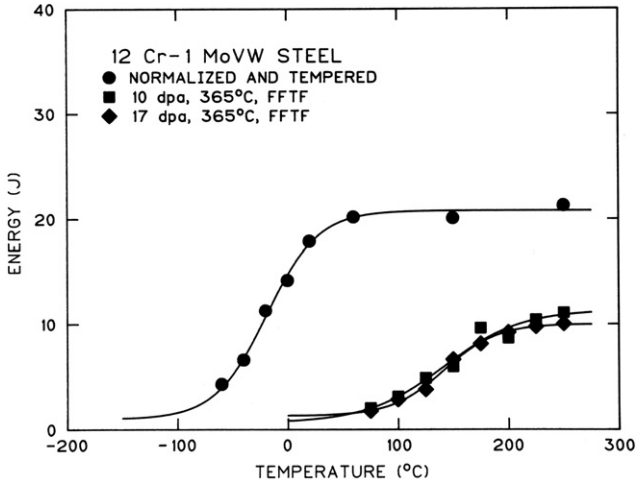

Fig. 4. Charpy impact curves for Sandvik HT9 (12Cr–1MoVW) in the unirradiated condition and after irradiation to 10 and 17 dpa at 365 °C in FFTF [11].

saturates (Fig. 3) [9]. The magnitude of the shift in the hardening regime varies inversely with irradiation temperature, similar to the variation in hardening.

Embrittlement in the irradiation-hardening temperature regime has been studied and discussed in detail [1]. In this paper, embrittlement at temperatures above the hardening regime will be examined and discussed. Observations where this occurs will be taken from the literature and from thermal aging experiments on unirradiated steels, and an explanation for the observations will be sought to determine the extent of this process and the effect it might have on the use of the steels for fusion applications.

2. Experimental materials and irradiation conditions

Several steels will be discussed in this paper (Table 1); these include the commercial steels modified 9Cr–1Mo, Sandvik HT9, EM10, EM12, and F17, and the reduced-activation steels F82H, EUROFER, and ORNL 9Cr–2WVTa [12,17,18]. All but F17 are primarily martensitic steels irradiated in the normalized-and-tempered condition. Normalization involves austenitizing to transform the

Table 1
Compositions of steels (wt%)

Steel	C	Cr	Mo	V	Nb	W	Ta	Mn	Si	Ni	N
Mod 9Cr–1Mo	0.086	8.44	0.89	0.24	0.08			0.37	0.16	0.11	0.05
Sandvik HT9	0.21	12.11	1.03	0.33	0.018	0.53		0.50	0.21	0.58	0.02
EM10	0.105	8.76	1.05					0.48	0.37		
EM12	0.086	9.58	1.91	0.28	0.41			0.92	0.37	0.12	
F17	0.056	17.27	0.01					0.36	0.35	0.09	0.017
F82H	0.093	7.50		0.14		2.01	0.02	0.17	0.16	0.02	0.006
9Cr–2WVTa	0.11	8.90		0.23		2.01	0.06	0.44	0.21		0.022
JLF-1	0.10	8.94		0.19		2.02	0.07	0.52	0.04	0.01	0.022
EUROFER	0.11	8.82		0.19		1.10	0.07	0.37	0.01	0.02	0.021

steel to austenite, after which it is air cooled or quenched in liquid to form martensite. Tempering is carried out at 750–780 °C for 0.25–1 h. The F17 is a high-chromium ferritic steel that does not transform to austenite on heating; it was cold-worked 20% followed by an 800 °C recrystallization treatment [17].

Matrix microstructures of normalized modified 9Cr–1Mo, EM10, which is basically unmodified 9Cr–1Mo (it is 'unstabilized' in that it does not contain vanadium and niobium as does modified 9Cr–1Mo), F82H, EUROFER, JLF-1, and 9Cr–2WVTa are 100% martensite. The HT9 is near 100% martensite, but it can contain a few percent (usually <5%) δ-ferrite, while EM12, which contains ≈2% of ferrite-stabilizing molybdenum, is a duplex steel with around 30% δ-ferrite and 70% martensite. The non-transformable F17 is 100% ferrite after the cold work and anneal treatment.

Before irradiation, the primary precipitate of normalized-and-tempered martensitic steels or the cold-worked-and-recrystallized F17 is chromium-rich $M_{23}C_6$, which is generally present on prior-austenite grain boundaries and martensite lath boundaries in the 100% martensitic steels, on prior-austenite grain boundaries, martensite lath boundaries, and martensite/δ-ferrite boundaries in the duplex steels, and on the ferrite boundaries of the ferritic steel. For steels containing vanadium, niobium, and/or tantalum (modified 9Cr–1Mo, HT9, EM12, F82H, EUROFER, JLF-1, and 9Cr–2WVTa), vanadium-, niobium-, and/or tantalum-rich MX precipitates are present in the matrix.

The steels discussed here were irradiated in several reactors. Tensile and Charpy specimens of modified 9Cr–1Mo and HT9 were irradiated in the Experimental Breeder Reactor (EBR-II) [12], and the F82H was irradiated in the High Flux Isotope Reactor (HFIR) [18,19]. Tensile and Charpy specimens of F17 were machined from wrapper tubes irradiated in the Phénix fast reactor; the EM10 and EM12 specimens were machined from unirradiated wrapper tubes and tubes irradiated in the Phénix fast reactor in the same experiment as the F17 [17].

3. Results and analysis

3.1. HT9 and modified 9Cr–1Mo steels

3.1.1. Experimental observations

Tensile [8–10] and Charpy specimens [12] of Sandvik HT9 and modified 9Cr–1Mo steels were irradiated in the EBR-II to 12–13 and 25–26 dpa at 390, 450, 500, and 550 °C. After irradiation at 390 °C, hardening occurred for modified 9Cr–1Mo (9Cr–1MoVNb) steel, but there was essentially no hardening at 450, 500, and 550 °C (Fig. 1) [8]. Based on the premise that irradiation hardening causes the embrittlement measured in an impact test, no embrittlement is expected after irradiation at 450, 500, and 550 °C. Indeed, no significant shift in DBTT (ΔDBTT) was observed for modified 9Cr–1Mo at these temperatures (Fig. 5) [12]. This contrasts to increases in DBTT of 52 and 54 °C at 390 °C for irradiations to 13 and 26 dpa, respectively. The ΔDBTTs at 390 °C reflect the hardening and saturation at 13 and 26 dpa, respectively, observed for yield stress and ultimate tensile strength [10].

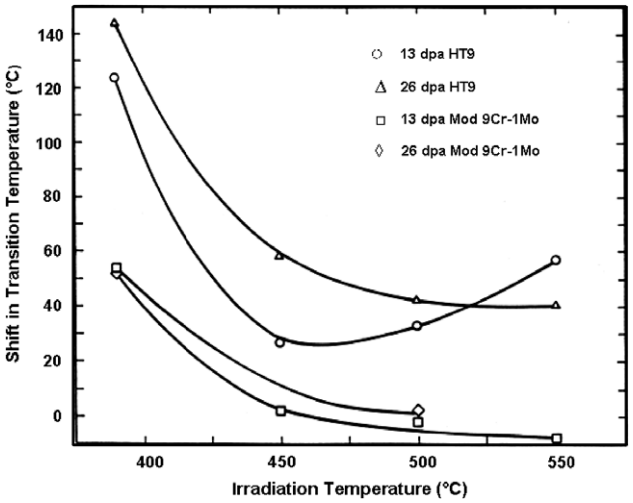

Fig. 5. Shift in ductile–brittle transition temperature of Sandvik HT9 and modified 9Cr–1Mo steels irradiated in EBR-II at 390, 450, 500, and 550 °C to 13 and 26 dpa [12].

The change in yield stress with irradiation temperature observed for HT9 (Fig. 3) [8] was similar to the observations on modified 9Cr–1Mo (Fig. 1) [9]. In this case, there was no difference in yield stress in the specimens irradiated in EBR-II at 390 °C to 13 and 25 dpa, indicating the expected saturation with fluence [10], and there was no hardening for the specimens irradiated at 450, 500, and 550 °C. There appeared to be a softening after the 25 dpa irradiation (Fig. 3). Rockwell hardness measurements on the Charpy specimens showed that hardening occurred only for the specimens irradiated at 390 °C [12], which agrees with the relative changes with irradiation temperature observed for the yield stress and ultimate tensile strength [8–10].

Despite there being no difference in yield stress for HT9 after 13 and 26 dpa at 390 °C, there was a 20 °C difference in ΔDBTT, where values of 124 and 144 °C were measured (Fig. 5). This difference in DBTT was originally assumed to be within the scatter of the data, thus indicating a saturation with dose [13], similar to observations on HT9 irradiated to 10 and 17 dpa at 365 °C in the (FFTF) (Fig. 4) [11]. However, as discussed below, this difference is now believed to be caused by irradiation-induced microstructural changes.

Although irradiation of the HT9 at 450, 500, and 550 °C did not cause an increase in yield stress from that for the unirradiated normalized-and-tempered value, this did not correlate with the observation on the ΔDBTT, which did not decrease to zero, as for modified 9Cr–1Mo, but it remained positive at all three temperatures (Fig. 5). For the high-dose irradiation, the shift was ≈60 °C at 450 °C, decreasing to around 40 °C at 550 °C [12].

3.1.2. Analysis of observations

An explanation for the difference in embrittlement behavior of HT9 and modified 9Cr–1Mo above the hardening temperature regime (Fig. 5) was sought in the precipitates in the steels [20], since this appears to be the only difference in normalized-and-tempered microstructures of the two steels [21,4,3]. The HT9 contains about twice as much carbon as modified 9Cr–1Mo, and as a result, it contains more carbide precipitate after tempering. Measurements of total precipitate extracted from the two steels in the normalized-and-tempered condition found 3.8 and 1.5 wt% in HT9 and modified 9Cr–1Mo, respectively [22]. The majority of precipitate in both steels was $M_{23}C_6$, with a small amount of MX. Larger amounts of larger precipitate particles were present on lath and prior-austenite grain boundaries in HT9 than in modified 9Cr–1Mo [22].

The larger amount of precipitate and its distribution in HT9 steel can be used to explain why ΔDBTT did not go to zero even though there was no irradiation hardening. Fracture in steels is generally initiated at carbide particles and/or inclusions [23,24]. The critical stress to propagate a crack is inversely proportional to crack length [23]. If it is assumed that fracture initiation occurs at an $M_{23}C_6$ particle (the large precipitate particles in the microstructure) and the crack length at initiation equals the diameter of a carbide particle, then fracture stress will decrease with increasing precipitate size.

Indications are that irradiation accelerates precipitate-particle coarsening during irradiation at 400–550 °C [21,4,3], thus causing a decrease in fracture stress and an increase in DBTT, even in the absence of hardening – or even in the presence of softening. The average $M_{23}C_6$ particle size in normalized-and-tempered HT9 is larger (or becomes larger faster) than that of modified 9Cr–1Mo because of the larger amount of carbon in HT9. After irradiation at 500 °C, considerably more coarsening has been observed for HT9 than modified 9Cr–1Mo [3]. Therefore, the fact that ΔDBTT for HT9 increased between 13 and 26 dpa at 390 °C and did not go to zero at 450–550 °C, even though hardening disappeared at these temperatures, can be attributed to irradiation-accelerated precipitate ($M_{23}C_6$) coarsening at the higher irradiation temperatures [20]. The minimum at ≈450 °C in the 13 dpa curve can also be attributed to precipitate coarsening. Coarsening kinetics increase with temperature. Thus, the larger precipitates at 500 and 550 °C after the 13 dpa irradiation have a larger embrittling effect. The observation that the ΔDBTT after 26 dpa at 550 °C is less than that after 13 dpa may indicate an approach to a balance between increased embrittlement due to increasing precipitate particle size and matrix softening due to the precipitate coarsening.

The conclusion that precipitation caused different relative irradiation effects on modified 9Cr–1Mo and HT9 above 390 °C is bolstered by examining the effect of low-temperature irradiation on the two steels. A very different relative effect was observed when the two steels were irradiated in HFIR to ≈10 dpa at ≈55 °C [25–27]. As opposed to the observations after irradiation at 390–550 °C in EBR-II where the ΔDBTT of HT9 was greater than that of modified 9Cr–1Mo, the ΔDBTT for the modified 9Cr–1Mo irradiated at the lower temperature was 135 °C compared to 55 °C for HT9 [25,26]. This occurred despite no large difference in hardening; similar increases in yield stress for the two steels were observed [27]. Although saturation was not reached at this low temperature, the results for the low-and high-temperature irradiations indicated that modified 9Cr–1Mo behaved as expected. That is, the shift in DBTT for modified 9Cr–1Mo decreased with increasing irradiation temperature, as expected, whereas the HT9 displayed the opposite effect.

A logical explanation for the difference in the two steels is that the increase in irradiation temperature from 55 to 390 °C caused a change in fracture behavior for one of the steels. Support for this was found by Gelles et al. [28,29], who observed δ-ferrite stringers on the cleavage fracture surface of HT9 irradiated in EBR-II at 390 °C, but not after irradiation at 55 °C in HFIR [29]. They concluded that the large ΔDBTT for HT9 at 390 °C was due to 'precipitation at δ-ferrite stringers' during irradiation at elevated temperatures, and these large carbide stringers acted as crack-nucleation sites [29]. Therefore, this change in fracture mode for HT9 at 390 °C due to localized precipitation at δ-ferrite–tempered martensite boundaries caused a larger increase in the DBTT at 390 °C than at 55 °C. At 390 °C, this precipitation effect occurs in conjunction with hardening. With increasing irradiation temperature, hardening ceases, but irradiation-accelerated coarsening of the precipitates causes the embrittlement in the absence of hardening.

The major differences in the two steels besides carbon concentration are the presence of Nb and N in modified 9Cr–1Mo but not in HT9, resulting in more MX in modified 9Cr–1Mo than HT9 [22]. Computational thermodynamics calculations with the JMatPro program [30] of the amount of the MX precipitate present after tempering at 760–780 °C predicted modified 9Cr–1Mo to contain 0.28 wt% of this matrix phase compared to 0.13 wt% for HT9. Therefore, an interaction between the displacement damage in the matrix with the larger amount of matrix MX of modified 9Cr–1Mo might cause the different behaviors at low temperatures. At high temperature, hardening due to displacement damage decreases, while at the same time the $M_{23}C_6$ particles on δ-ferrite/martensite boundaries of HT9 grow to much larger sizes than in modified 9Cr–1Mo, eventually causing the relative effect observed at low temperatures to reverse.

This explanation of the temperature effect is consistent with the above explanation for the difference between the impact behavior of modified 9Cr–1Mo and HT9 steels at 390–550 °C. Because of irradiation-enhanced diffusion at 390 °C in EBR-II, precipitates coarsen at δ-ferrite-martensite interfaces of HT9 (no δ-ferrite is present in modified 9Cr–1Mo), and these precipitates can also cause a change in fracture behavior in the presence of hardening, as observed. No such diffusion-assisted precipitates would be expected after 10 dpa at 50 °C but would only begin to form at the higher irradiation temperatures. Thus, although the ΔDBTT of HT9 at 50 °C is about half as large as the ΔDBTT of modified 9Cr–1Mo, the change in microstructure for HT9 makes the ΔDBTT of the latter steel over twice that of the former at higher temperatures.

The explanation involving δ-ferrite for the different relative behavior of modified 9Cr–1Mo and HT9 at 55 and 390 °C is supported by work of Anderko and Schäfer [31,32] who showed that δ-ferrite in 12Cr steels does not by itself cause early cleavage, as suggested by other investigators [33]. In fact, the relatively soft δ-ferrite can improve the ductility and toughness [32]. Rather, it was concluded that fracture initiated at $M_{23}C_6$ precipitates on δ-ferrite/martensite interfaces [31,32]. Therefore, the fact that δ-ferrite stringers were not observed by Hu and Gelles on the HT9 fracture surface after the 55 °C irradiation [29] suggests that the absence of interface precipitation and the presence of smaller particles at 55 °C may be responsible for the inherently better behavior of HT9 than modified 9Cr–1Mo at lower temperatures. At higher temperatures where irradiation-accelerated precipitation and precipitation coarsening occur, the carbides on the δ-ferrite/martensite interface and prior-austenite and lath boundaries cause a larger ΔDBTT for HT9 than modified 9Cr–1Mo.

In addition to the growth of $M_{23}C_6$ precipitates, chromium-rich α′ can precipitate during irradiation or during thermal aging. After irradiation of the two steels in the Fast Flux Test Facility (FFTF) at 420 °C, α′ was observed in the HT9 but not in the 9Cr steel [4]. This agrees with thermodynamics calculations with JMatPro, which indicate that α′ is stable below about 440 °C in HT9 and below about 405 °C for modified 9Cr–1Mo. Since the temperatures of interest are above 440 °C, little or no α′ should be present. Also,

as discussed for F17 in the following section, α′ formation is accompanied by hardening, which was not observed for HT9 at 450–550 °C (Fig. 3), indicating that this phase is probably not playing a major role in the observed behavior.

One way α′ might play a role without causing measurable hardening is if several percent δ-ferrite is present. Thermodynamics calculations indicate δ-ferrite is enriched in chromium; this could increase the amount of α′ in that phase and increase the maximum temperature at which it forms. Hardening of δ-ferrite by α′ might then enhance crack nucleation in the $M_{23}C_6$ at the δ-ferrite/tempered martensite boundary without leading to measurable hardening in the overall alloy. However, even in this case it is doubtful that α′ will play a significant role, since the embrittlement also occurs at 500 and 550 °C, where calculations indicate no α′ should form, even in the chromium-enriched δ-ferrite.

3.2. F17, EM10, and EM12 steels irradiated in Phénix

3.2.1. Experimental observations

Gilbon et al. investigated EM10, EM12, and F17 steels irradiated over the range ≈390 to 540 °C up to 100 dpa in the Phénix fast reactor [17]. For all three steels, impact tests indicated the largest effects occurred for the steels irradiated at 390 °C where hardening occurs (Fig. 6).

The most embrittlement occurred for F17, where the DBTT after the 390 °C irradiation reached 280 °C, as opposed to −50 °C before irradiation (ΔDBTT = 330 °C). In addition to embrittlement at the lowest irradiation temperature, a significant ΔDBTT was observed over the entire irradiation-temperature range. Even for irradiation at 540 °C, the ΔDBTT was ≈110 °C. Fig. 6 is the average of two irradiated F17 wrapper tubes [17], and in Fig. 7, the DBTTs for the two wrappers are shown along with data for unirradiated steel thermally aged for 10 000 h. Except for the low-temperature end of the data, the impact behavior for the irradiated and the aged steels is similar.

Considerably fewer irradiated EM10 and EM12 specimens were tested, and both steels developed smaller ΔDBTTs than F17 (Fig. 6) [17]. A small ΔDBTT was observed for EM10 at around 400–440 °C. Between 440 and 500 °C, there was essentially no change in DBTT, but above about 510 °C there was again a slight increase. For EM12, a slightly larger DBTT was observed for a limited number of specimens. In this case, embrittlement occurred for tests at 400, 450, 500, and 520 °C, although there may have been slightly less at the intermediate temperature of 450 °C.

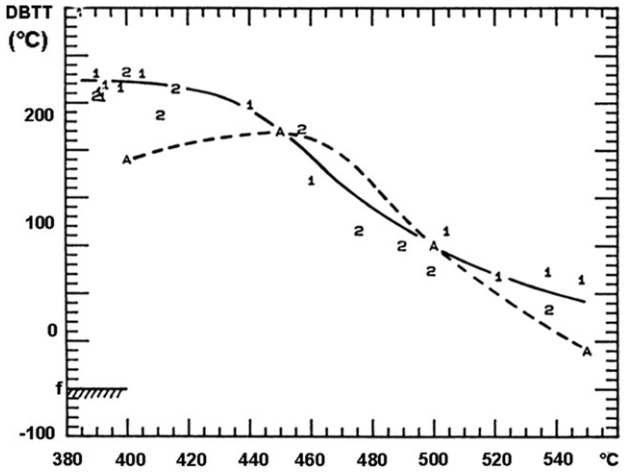

Fig. 7. Ductile–brittle-transition temperature as a function of irradiation and aging temperature for specimens taken from two F17 steel wrappers (1 and 2) irradiated in the Phénix reactor compared to the steel thermally aged for 10 000 h (A) [17]. Unirradiated value is indicated as 'f'.

Results of tensile tests were reported for EM10 and F17, but not EM12 [17]. For both steels, hardening, as measured by an increase in yield stress and ultimate tensile strength, occurred at the lowest irradiation temperatures – about 390–440 °C (Fig. 8). At higher irradiation temperatures, the strength of EM10 approached the strength of the unirradiated steel. For F17, however, strength of irradiated steel remained above that for unirradiated steel to about 540 °C.

The yield stress and ultimate tensile strength of the irradiated F17 steel was compared to specimens thermally aged for 2000 h at 450, 500, and 550 °C. Again, the irradiated properties approached those for the aged material (Fig. 8) [17].

3.2.2. Analysis

The observations on F17 steel were explained by Gilbon et al. as caused by formation of a fine distribution of α' precipitate [17]. In both the thermally aged and the irradiated steel, a high number density of small α' precipitates was observed at 400 °C, with the number density decreasing and size increasing with increasing temperature. Precipitate particles in the irradiated steel were larger than in the aged material, indicating irradiation-accelerated growth. Up to about 460 °C, α′ precipitation in the irradiated steel

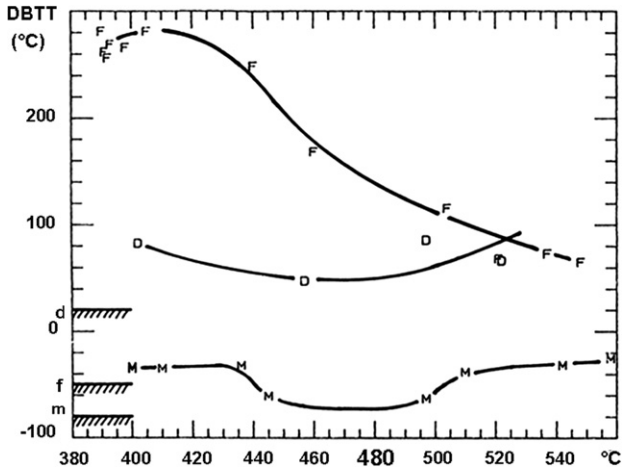

Fig. 6. Ductile–brittle-transition temperature as a function of irradiation temperature for EM10 (M), EM12 (D), and F17 (F) steels irradiated in the Phénix reactor [17]. Unirradiated values are indicated as 'd', 'f', and 'm'.

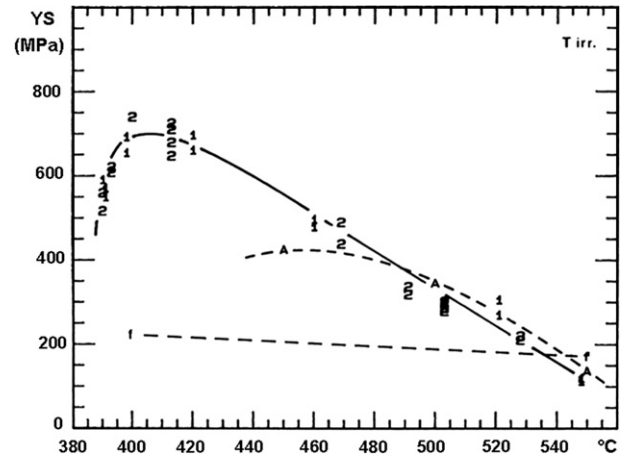

Fig. 8. Yield stress as a function of irradiation and aging temperature for the two F17 steel wrappers (1 and 2) irradiated in the Phénix reactor compared to the steel thermally aged for 10 000 h (A) and as-heat-treated (f) [17].

was quite uniform, but it became 'patchy at temperatures above 500 °C' [17]. No α′ was observed in the aged specimen at 550 °C, but instead, sigma phase was observed along grain boundaries. Sigma was also found in the steel irradiated at 540 °C.

Observations on the α′ precipitate were in good agreement with the hardening (Fig. 8) and the increase in DBTT (Fig. 7). Although the results indicated that irradiation hardening played a role in the embrittlement for irradiation at 390 °C – and presumably at lower temperatures – between about 440 and 520 °C, the increase in DBTT was caused by α′, which precipitates when the steel is heated to this temperature, although irradiation probably accelerated precipitation.

For the limited number of specimens of irradiated EM12, the ΔDBTT for the duplex microstructure irradiated at around 400 °C was attributed to irradiation hardening [17]. However, for specimens irradiated at the higher temperatures, a distribution of χ-phase was identified. This phase had a different distribution in the tempered martensite and the δ-ferrite (Fig. 9).

Calculations with JMatPro indicate that χ-phase is not an equilibrium phase. Instead, Laves is predicted to be present at equilibrium. This must mean that χ-phase is an irradiation-induced phase (i.e., the equilibrium phase under irradiation conditions), or it is a metastable phase favored by kinetic considerations, and it will eventually be replaced by Laves phase. χ-Phase is calculated to form if the calculations are made under conditions that do not allow Laves to form. Chi, like Laves, is an Fe–Mo–Cr-rich intermetallic phase. Based on photomicrographs presented [17], it appears that the reason for ΔDBTTs similar to those at the lowest temperature could be attributed to the same mechanism as postulated above for HT9.

The little or no change in properties of the EM10 is in agreement with that for modified 9Cr–1Mo. As pointed out above, EM10 is unstabilized (unmodified) 9Cr–1Mo steel, since it does not contain the Nb, V, and N that are present in modified 9Cr–1Mo. Gilbon et al. [17] stated that there was essentially no change in the precipitate distribution in EM10 before and after irradiation.

3.3. F82H steel

3.3.1. Experimental observations

One-third-size pre-cracked Charpy (PCVN), Charpy V-notch (CVN), and 0.18 T disk-compact fracture-toughness (DC(T)) specimens of F82H steel were irradiated in HFIR to ≈3–5 and 20 dpa at 300–500 °C [18,19]. The PCVN, CVN, and DC(T) specimens were tested to determine the transition temperature before and after irradiation. Tensile specimens were irradiated to 4.7–4.8 and 20 dpa at 300 and 500 °C and tested at −100 °C, room temperature, and at the irradiation temperature [18].

A large increase in yield stress was observed after irradiation at 300 °C to 4.7 and 20 dpa, with most of the change occurring for the 4.7 dpa irradiation (Fig. 10(a)). There was only a slight further increase after 20 dpa. Irradiation at 500 °C to 4.8 and 20 dpa had no effect on the yield stress [18].

Fracture toughness transition temperature shifts were evaluated with the master curve methodology [18], and shifts showed a pronounced effect of irradiation temperature (Fig. 10(b)). The largest effect was for the lowest temperature irradiations, with the shift decreasing with increasing temperature. Unexpectedly, there was a shift of 33 °C for the 5 dpa CVN specimen irradiated

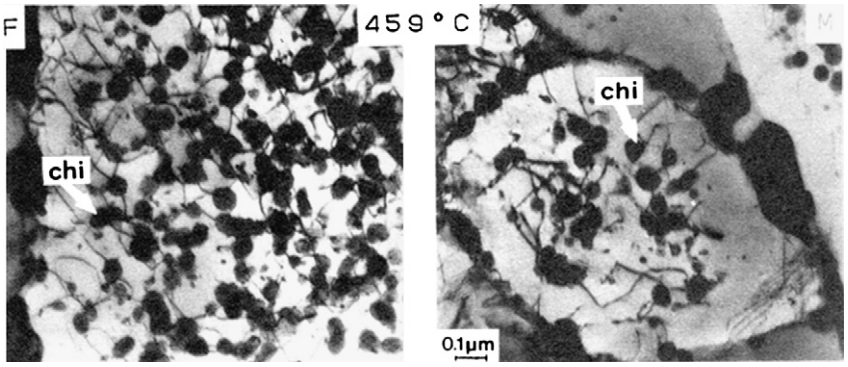

Fig. 9. Transmission electron microscopy photomicrographs of χ-phase in (a) δ-ferrite and (b) tempered martensite of EM12 steel irradiated in the Phénix reactor to ≈40 dpa [17].

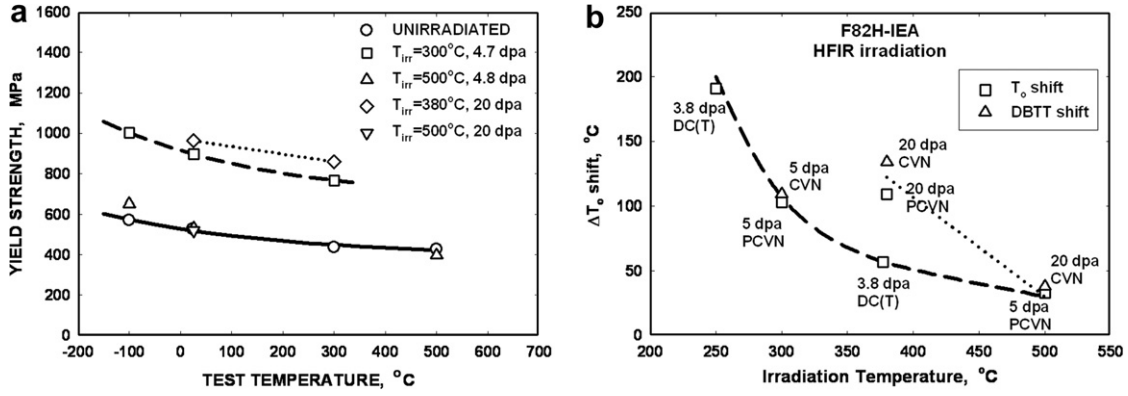

Fig. 10. The (a) yield stress as a function of test temperature and (b) transition temperature as a function of irradiation temperature for F82H irradiated in HFIR over the range 250–500 °C [18].

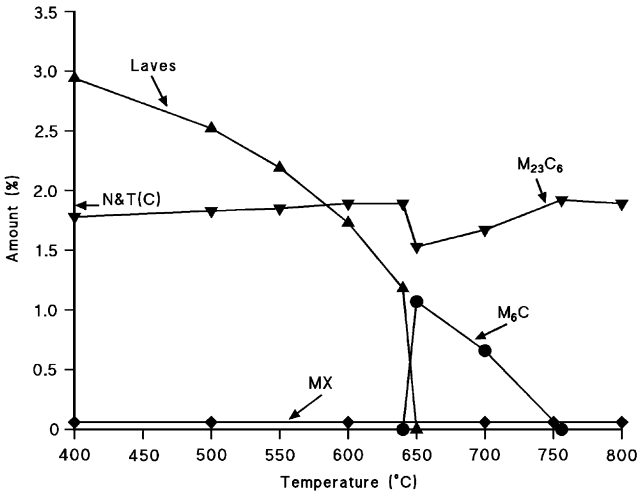

Fig. 11. Equilibrium amounts of precipitates in F82H steel over the range 400–800 °C, as calculated by the computational thermodynamics program JMatPro. The total amount of precipitate calculated for the steel tempered at 750 °C is indicated as N&T (C).

at 500 °C, and this was corroborated by a 38 °C shift for the 20 dpa CVN specimen [19].

3.3.2. Analysis

After irradiation at 500 °C in the absence of irradiation hardening, the increase in transition temperature for the F82H can also be traced to irradiation-accelerated precipitation. In this case, the precipitate is concluded to be Laves phase [$(Fe,Cr)_2W$]. For normalized-and-tempered F82H tempered at 750 °C, the major precipitate is chromium-rich $M_{23}C_6$; a small amount of MX is also present. Thermodynamics calculations with JMatPro predict 1.9 wt% $M_{23}C_6$ and 0.06 wt% MX form at 750 °C, along with 0.075 wt% tungsten-rich M_6C (Fig. 11). Laves phase is predicted to be stable below ≈650 °C. The calculations indicate an abrupt cutoff temperature for Laves: at ≈640 °C, 1.22% Laves is predicted, after which it drops to zero by ≈650 °C. However, tungsten-rich M_6C is predicted to form below 767 °C and increase to 1.15% at 650 °C, where it then drops abruptly to zero at 639 °C. The Laves and M_6C curves constitute an essentially continuous curve of tungsten-rich precipitates, with Laves predicted to form up to 640 °C and M_6C forming at the higher temperature until it becomes unstable at 766 °C (Fig. 11).

Shiba thermally aged tensile and Charpy specimens of F82H for 1000, 3000, 10000, and 30000 h at 400 (aged 30000 h only), 500, 550, 600, and 650 °C [34,35]. Although aging caused a reduction in room-temperature strength that was quite large at the highest temperatures and longest times (Fig. 12(a)), there was an adverse effect on impact properties (Fig. 12(b)). The largest strength decreases occurred at 600 and 650 °C; at 650 °C, a 33% decrease occurred after 30000 h. Despite this large decrease in strength at 650 °C, the largest increase in Charpy DBTT (105 °C) also occurred at this temperature after 30000 h. The DBTT also increased at the other temperatures, with the magnitude of the increase decreasing with decreasing aging temperature. The change was relatively small at 400 and 500 °C, even after 30000 h.

Chemical analysis of the extracted precipitates from normalized-and-tempered and thermally aged specimens revealed an increase in W, Fe, and Cr with aging time and temperature (Fig. 13). For aging up to 3000 h, the total amount of precipitate increased at 600 and 650 °C. After 10000 and 30000 h, the largest increase in the amount of precipitate occurred at 600 °C. The largest elemental increases involved tungsten, iron, and chromium, all three of which are major components of Laves phase. X-ray diffraction and EDS analysis of extracted precipitates verified the presence of Laves phase after aging at 500, 550, 600, and 650 °C. Contrary to the JMatPro calculations, some M_6C was detected by X-ray diffraction of extracted precipitate from specimens aged 10000 h at 500, 550, and 600 °C. Primary constituents in both M_6C and Laves phase are W, Fe, and Cr. If JMatPro equilibrium calculations are valid, one explanation for M_6C is that it is a metastable precursor of Laves phase. A second, and more probable, possibility can be based on the calculated curve for Laves and M_6C in Fig. 11, namely, that a small amount of the M_6C formed during tempering at 750 °C was retained when cooled after tempering, and equilibrium had not yet been established after aging 10000 h. Another discrepancy between calculations and experiments is the identification of Laves phase instead of M_6C in extracted precipitates from specimens aged at 650 °C. This observation indicates that the transition from Laves phase to M_6C occurs at a higher temperature than the 640 °C calculated by JMatPro (Fig. 11).

When the total amount of precipitate calculated with JMatPro (the sum of the three curves in Fig. 11) is compared to the measured precipitate after 30000 h, the effect of kinetics versus equilibrium is evident (Fig. 14). Equilibrium was apparently reached at 650 °C, and it is being approached after aging 30000 h at 600 °C. Significant amounts of precipitate formed at 550 °C, but because of the reduced kinetics, very little formed at 400 and 500 °C. Much more will form at longer aging times. However, from observations on the increase in transition temperature that occurred during irradiation of F82H at 500 °C in HFIR compared to that observed during thermal aging, it is concluded that irradiation accelerates precipitation kinetics, thus causing embrittlement, even though there was no hardening.

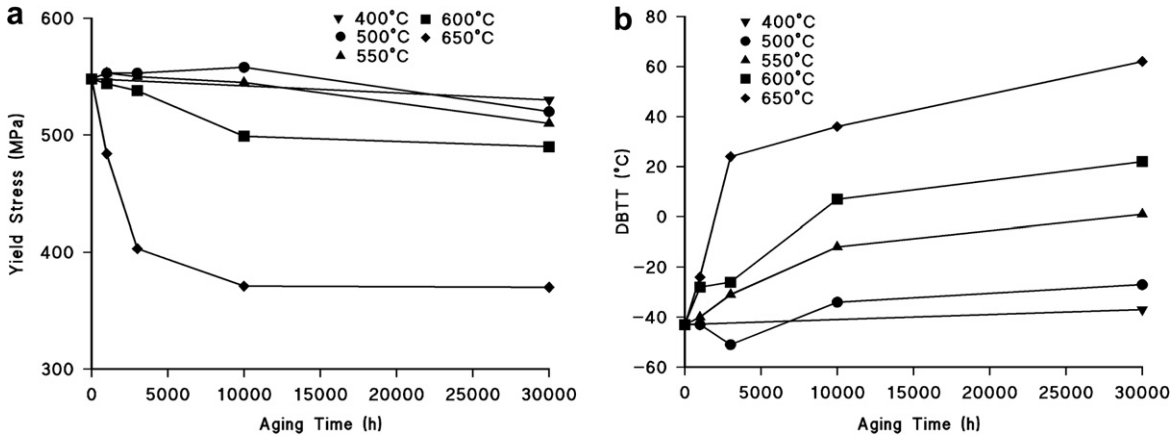

Fig. 12. The (a) yield stress and (b) ductile–brittle-transition temperature of F82H steel as a function of aging time at 500, 550, 600, and 650 °C [34,35].

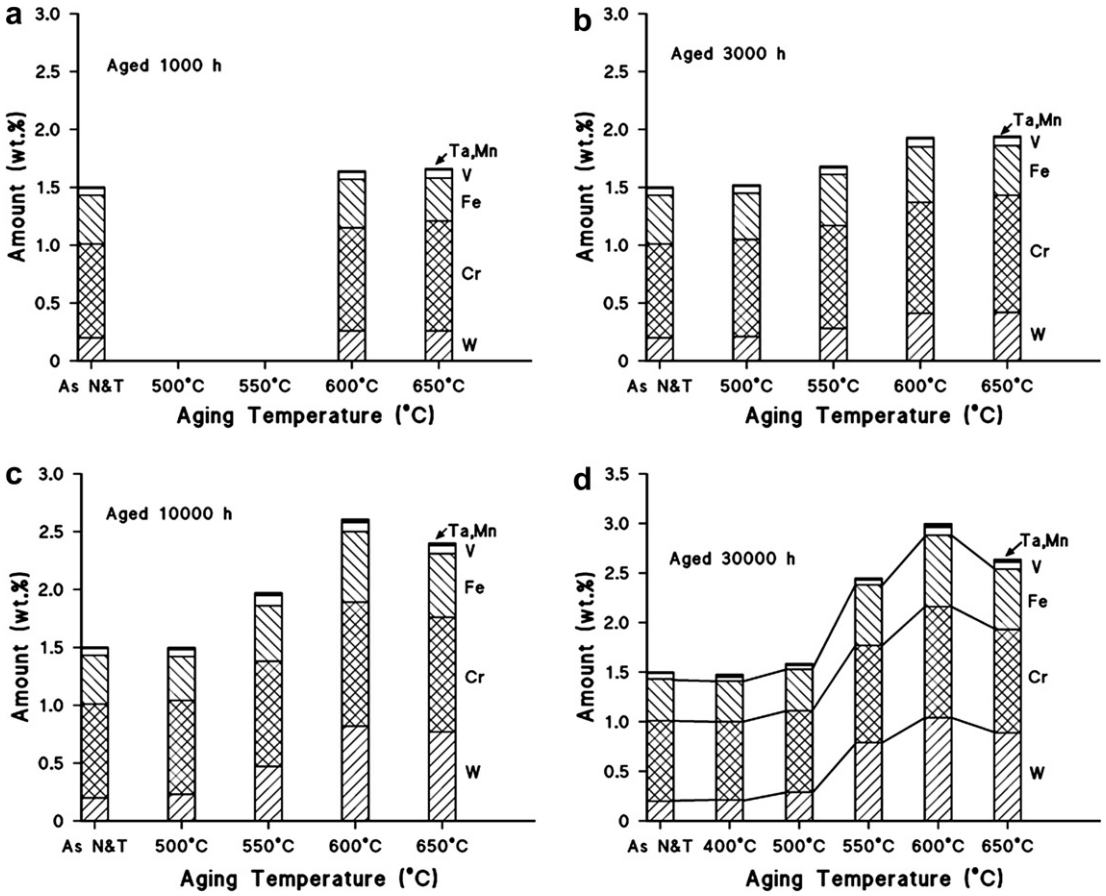

Fig. 13. Amount of W, Cr, Fe, V, Ta, and Mn in extracted precipitate from F82H steel aged at 400, 500, 550, 600, and 650 °C for (a) 1000, (b) 3000, (c) 10000, and (d) 30000 h [34,35].

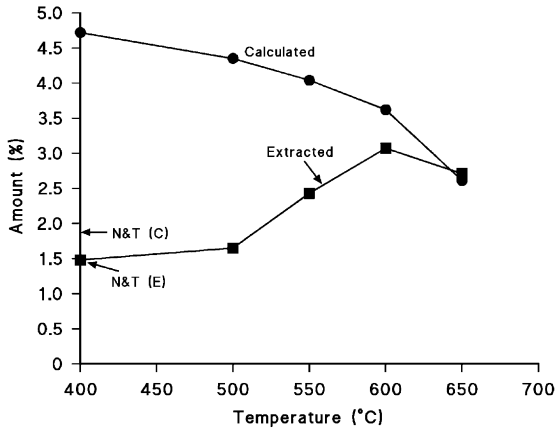

Fig. 14. A comparison of the amount of extracted $M_{23}C_6$, MX, Laves, and M_6C phases with that calculated to be present at equilibrium in normalized-and-tempered F-82H steel thermally aged 30000 h at 400, 500, 550, 600, and 650 °C. The amounts extracted and calculated for the steel tempered at 750 °C are indicated by N&T (E) and N&T (C), respectively.

4. Discussion

For HT9, EM12, F17, and F82H steels, the observations of embrittlement in the absence of irradiation hardening appeared to be caused by precipitation that occurred during irradiation, with somewhat different precipitates forming in each case. These observations raise the following questions. Why is HT9 (12Cr–1MoVW) affected by the precipitation of $M_{23}C_6$? Why is modified 9Cr–1Mo (9Cr–1MoVNb) not affected by $M_{23}C_6$ precipitation? Why is F82H affected by Laves phase? Why is modified 9Cr–1Mo not affected by Laves phase?

To answer these questions, the computational thermodynamics program JMatPro [30] was used to calculate the stable phases in these steels. Table 2 shows the amounts of $M_{23}C_6$ and Laves phase predicted for each steel discussed in this paper.

The calculations show clearly that HT9 contains by far the most $M_{23}C_6$, about twice that of modified 9Cr–1Mo steel over the range 500–650 °C. This follows because this steel contains twice as much carbon, and it agrees with the experimental observations from precipitates extracted from the steels [22]. The calculations are in agreement with the mechanism for the observed behavior suggested above.

When F82H and modified 9Cr–1Mo are compared, both steels contain similar amounts of $M_{23}C_6$. However, F82H is calculated to have almost five times more Laves phase as modified 9Cr–1Mo at 400 °C and 25 times more at 550 °C (Table 2). Laves phase is stable in F82H up to at least 640 °C, but it is not stable above ≈560 °C in modified 9Cr–1Mo. For modified 9Cr–1Mo, JMatPro indicates that instead of molybdenum-rich Laves phase forming at 560 °C, molybdenum-rich μ-phase forms between ≈560 and 480 °C, below which Laves forms. Both phases are variations of $(Fe,Cr)_2Mo$, but with different amounts of molybdenum; μ contains ≈46% compared to ≈52% for Laves.

The difference in the two steels arises because F82H contains tungsten and modified 9Cr–1Mo contains molybdenum. F82H and other reduced-activation steels were developed by patterning them after modified 9Cr–1Mo, where tungsten was chosen to replace molybdenum because both are Group VI elements in the periodic table. An atom-for-atom replacement was made, which

Table 2
Precipitate amounts in steels calculated by computational thermodynamics (wt%)

Steel	$M_{23}C_6$				Laves			
	500 °C	550 °C	600 °C	650 °C	500 °C	550 °C	600 °C	650 °C
Mod 9Cr–1Mo	1.94	1.93	1.92	1.80	0.55	0.10	0	0
Sandvik HT9	3.87	3.87	3.86	3.83	0.85	0.55	0.15	0
EM10	2.04	2.04	2.04	2.04	0.56	0.25	0	0
EM12	0.89	0.74	0.69	0.66	3.28	2.45	1.92	0
F17	0.99	0.99	0.99	0.99	0	0	0	0
F82H	1.89	1.90	1.91	1.80	2.55	2.25	1.77	0.89
EUROFER	2.05	2.10	2.15	2.10	1.0	0.60	0.20	0

required 2 wt% W for 1 wt% Mo, since the atomic weight of tungsten is about twice that of molybdenum. Despite the two steels containing similar atom fractions of the two elements, the calculations indicate that the tungsten-containing steel forms much more $(FeCr)_2W$ than the molybdenum-containing steel forms $(FeCr)_2Mo$, and it forms it over a wider temperature range.

Thermal aging studies on modified 9Cr–1Mo steel at 482–704 °C to 50 000 h found that Laves phase precipitation resulted in sharp increases in DBTT at 482, 538, and 593 °C with little change in strength [36]. The increases reached a maximum after aging 25 000 h. On the other hand, irradiation studies of the modified 9Cr–1Mo and HT9 indicated that Laves was suppressed by irradiation at 300–615 °C [37,38]. Laves phase was also found in irradiated reduced-activation steels 7Cr–2WVTaN, 9Cr–2WVTaN, 9Cr–2WVTaTiN, and 12Cr–2WVTaN irradiated to 30–36 dpa at 425 °C in FFTF [39–42], and 8Cr–2WVTaB (an earlier version of F82H) irradiated to 37 dpa at 750 °C in FFTF [43]. These observations in conjunction with the thermodynamics calculations indicate that that the presence of tungsten in the reduced-activation steels enhances Laves precipitation relative to a similar atom fraction of molybdenum.

Embrittlement of EM12 was attributed to the formation of χ-phase [17]. This steel is calculated to contain even more Laves phase at 500 °C (3.28%) than F82H (Table 2) because the steel contains 1.91% Mo, which on an atom-for-atom comparison with tungsten is equivalent to ≈4% W. The JMatPro calculations do not indicate the presence of chi, a complex body-centered-cubic phase with a nominal composition $Fe_{35}Cr_{12}Mo_{10}C$, which, with the exception of carbon, is the same combination of elements expected in Laves. However, as suggested above, the difference between observations and calculations can mean either χ-phase is an irradiated-induced phase or is a metastable phase favored by kinetics and will eventually be replaced by Laves phase.

Embrittlement of F17 above the temperature where irradiation hardening occurs can be explained by the formation of α'. In this case, the precipitate hardens the matrix. Embrittlement caused by this precipitate in aged high-chromium ferritic steels, termed '475 °C embrittlement', has been known for some time [44].

Embrittlement of HT9, F82H, and EM12 steels appears to be associated with $M_{23}C_6$, Laves, and χ-phases, respectively, and the mechanism by which embrittlement occurs was suggested to be caused by large precipitates that act as crack-nucleation sites [20,28,29].

In the HFIR experiment containing the F82H–IEA heat that was irradiated to 5 and 20 dpa at 500 °C [18,19], the F82H–IEA with a different heat treatment (F82H–HT2), F82H weld metal, and the reduced-activation steels ORNL 9Cr–2WVTa and JLF-1 were also irradiated at 500 °C (Table 3) [45]. The latter two steels have compositions only slightly different from F82H (Table 1). All of these materials had a positive ΔDBTT, although, except for the weld metal, the other materials had a smaller ΔDBTT after the 5 dpa irradiation at 500 °C than the F82H–IEA heat. Laves phase in an amount similar to that in F82H is calculated to form in all of these tungsten-containing steels.

The objective of the different heat treatment for F82H was to obtain a smaller prior-austenite grain size than the large grain size of F82H–IEA. After normalizing at 920 °C instead of 1050 °C, the estimated ASTM grain size number increased from 3.3 to 6.5, corresponding to average grain sizes of ≈114 and ≈38 μm, respectively. The ORNL 9Cr–2WVTa and JLF-1 steels had ASTM grain-size numbers of 6, corresponding to ≈45 μm. They had smaller ΔDBTTs than the F82H–IEA, although they were somewhat larger than F82H–HT2 (Table 3).

Laves phase forms preferentially on prior-austenite grain boundaries, but the amount of Laves does not depend on grain size. Therefore, if ΔDBTT at 500 °C is caused by Laves phase, the difference in the F82H with different heat treatments could be the result of the different grain sizes, assuming all else remains the same. If most of the Laves forms on prior-austenite grain boundaries, then a smaller grain size would provide a larger surface area for heterogeneous nucleation. This should result in a larger number of smaller precipitates, which could explain the observations based on the crack-nucleation mechanism proposed previously [20,28,29].

Thermodynamics calculations indicate that the amount of Laves phase in the reduced-activation steels at 500 °C depends mainly on tungsten content, and since ORNL 9Cr–2WVTa and JLF-1 contain 2% W similar to the F82H, similar amounts of Laves are predicted for these steels as for F82H. The ORNL 9Cr–2WVTa and JLF-1 have similar compositions, and they have similar prior-austenite grain sizes, which are smaller than that of F82H–IEA. The ΔDBTTs for the two steels at 500 °C are similar, and somewhat higher than for F82H–HT2 and about half that of F82H–IEA (Table 3).

With time at temperature or for higher irradiation doses, the Laves phase precipitation will be completed, and the particles will coarsen. How this will affect the toughness needs to be determined by long-time thermal aging and/or higher-dose irradiation experiments. No information is available on the microstructure of the weld metal specimen.

Reduced-activation EUROFER steel developed in Europe has a composition similar to ORNL 9Cr–2WVTa and JLF-1, but with 1% W instead of 2% (Table 1) [46]. Thermodynamics calculations indicate that only about 1% Laves phase will form at 500 °C in EUROFER, compared to ≈2% for F82H (Table 2). At 600 °C, only about 0.25% Laves is expected. Given the reduced amount of Laves in EUROFER, it should experience less embrittlement at higher irradiation temperatures than the steels with 2% W.

Table 3
Shift in transition temperature of steels irradiated in HFIR at 500 °C

Material	Dose (dpa)	DBTT (°C)	ΔDBTT (°C)	Grain size No.
F82H–IEA	5	−54	30	3.3
	20	−46	38	
F82H (HT #2)	5	−92	9	6.5
F82H Weld Metal	5	−37	46	–
ORNL 9Cr–2WVTa	5	−78	16	6
JLF-1	5	−66	19	6

In addition to embrittlement in the absence of irradiation hardening caused by irradiation-accelerated precipitation, embrittlement in the absence of commensurate irradiation hardening was previously observed on modified 9Cr–1Mo and HT9 steels and these steels with 2% Ni. In that case, embrittlement was attributed to helium formed during irradiation [47,48]. To explain the embrittlement, it was proposed that a microcrack source for fracture initiation could be helium-containing bubbles on a prior-austenite grain boundary, on a martensite lath boundary (subgrain boundary), or at a precipitate/matrix interface [48,49]. Examples of bubbles on boundaries were observed at temperatures where hardening occurs and at higher temperatures where no hardening occurs [49], leading to the conclusion that studies to determine helium effects should be extended to temperatures above the irradiation-hardening temperature, ≈425 °C. Because of the irradiation-accelerated precipitation presented in this paper, a similar conclusion now applies to the irradiation of the 9–12% Cr ferritic/martensitic steels used in nuclear applications – fission or fusion – even in the absence of large quantities of helium.

Recently, Odette and co-workers [50,51] discussed fracture under similar circumstances to those presented in this paper, which they labeled non-hardening embrittlement (NHE). They proposed a fracture mechanism similar to the mechanism proposed in this paper and that proposed in the previous papers on helium effects [48,49]. To describe the behavior, Odette et al. state that a 'multiscale model was developed, which has as its underpinning a model proposed by Ritchie et al. [52] that is based on the observation that cleavage occurs by the propagation of microcracks emanating from brittle trigger-particles, like large grain boundary carbides. . .' They write that, 'Local stress–strain concentrations due to incompatible matrix particle deformation cause some of the brittle ceramic trigger-particles to crack'. The importance of this behavior to structures such as the first wall of future fusion reactors was emphasized [50].

5. Summary and conclusions

In the past, radiation-effects studies in ferritic/martensitic steels have focused primarily on temperatures where irradiation hardening occurs (below 425–450 °C) and where hardening is accompanied by embrittlement caused by a reduction in toughness. Although embrittlement in the absence of hardening was observed that was attributed to helium effects, other observations of embrittlement of irradiated steels in the absence of irradiation hardening have received relatively little attention. In this paper, examples of irradiated steels that were embrittled in the absence of irradiation hardening were analyzed, and the embrittlement was attributed to irradiation-enhanced precipitation. Precipitates that were concluded to cause the observed behavior varied for the different steels and included $M_{23}C_6$ in Sandvik HT9, α' in F17 ferritic steel, χ-phase in EM12, and Laves phase in F82H. The observed effects were explained by postulating irradiation-enhanced or irradiation-induced precipitation and/or irradiation-enhanced precipitate coarsening that produced large precipitates that act as crack nuclei for fracture initiation.

The examples of embrittlement due to irradiation-enhanced or irradiation-induced precipitation cited were for relatively low fluences (<30 dpa) or relatively low temperatures (500 °C). In cases of the low fluences (relatively short thermal exposure times) and relatively low temperatures, precipitation may be incomplete, and the ultimate effect of the precipitates on properties has yet to be determined. Therefore, a need exists for high-dose irradiations at higher temperatures (500–600 °C).

Of the steels discussed, F82H is of most interest currently, since it is a leading candidate for structural applications in future fusion reactors. Irradiation in HFIR to 5 and 20 dpa at 500 °C indicated a moderate increase in transition temperature. However, thermal aging experiments demonstrated a large effect of Laves phase precipitation on the ductile–brittle transition temperature; a ΔDBTT of ≈105 °C occurred when aged 30 000 h at 650 °C. This increase occurred despite the yield stress decreasing 33% (≈180 MPa). Because the equilibrium amount of precipitate increases with decreasing temperature, a larger effect is expected at 500 and 550 °C, thus emphasizing the need for high-dose irradiation tests at these temperatures.

Computational thermodynamics calculations were used to analyze equilibrium phases for the steel compositions of interest. Such analyses can predict the amounts of precipitate expected. They can also be used to determine compositional variations for a particular steel to minimize the effect of precipitation on properties during irradiation or elevated-temperature exposure.

References

[1] R.L. Klueh, D.R. Harries, High-Chromium Ferritic and Martensitic Steels for Nuclear Applications, American Society for Testing and Materials, West Conshohocken, Pennsylvania, 2001.
[2] V.S. Agueev, V.N. Bykov, A.M. Dvoryashin, V.N. Golovanov, E.A. Medvendeva, V.V. Romaneev, V.K. Sharmardin, A.N. Vorobiev, in: N.H. Packan, R.E. Stoller, A.S. Kumar (Eds.), Effects of Radiation on Materials: 14th International Symposium, ASTM STP 1046, vol. I, American Society for Testing and Materials, Philadelphia, 1989, p. 98.
[3] P.J. Maziasz, R.L. Klueh, J.M. Vitek, J. Nucl. Mater. 141–143 (1986) 929.
[4] J.J. Kai, R.L. Klueh, J. Nucl. Mater. 230 (1996) 116.
[5] D.S. Gelles, J. Nucl. Mater. 212–215 (1994) 714.
[6] E.A. Little, L.P. Stoter, in: H.R. Brager, J.S. Perrin (Eds.), Effects of Irradiation on Materials: 11th Conference, ASTM STP 782, American Society for Testing and Materials, Philadelphia, 1982, p. 207.
[7] C. Wassilew, K. Herschbach, E. Materna-Morris, K. Ehrlich, in: J.W. Davis, D.J. Michel (Eds.), Ferritic Alloys for Use in Nuclear Energy Technologies, The Metallurgical Society of AIME, Warrendale, PA, 1984, p. 607.
[8] R.L. Klueh, J.M. Vitek, J. Nucl. Mater. 132 (1985) 27.
[9] R.L. Klueh, J.M. Vitek, J. Nucl. Mater. 137 (1985) 44.
[10] R.L. Klueh, J.M. Vitek, J. Nucl. Mater. 182 (1991) 230.
[11] R.L. Klueh, D.J. Alexander, in: R.E. Stoller, A.S. Kumar, D.S. Gelles (Eds.), Effects of Radiation on Materials: 15th International Symposium, ASTM STP 1125, American Society for Testing and Materials, Philadelphia, 1992, p. 1256.
[12] W.L. Hu, D.S. Gelles, in: F.A. Garner, C.H. Henager Jr., N. Igata (Eds.), Influence of Radiation on Material Properties: 13th International Symposium (Part II), ASTM STP 956, American Society for Testing and Materials, Philadelphia, 1987, p. 83.
[13] R.L. Klueh, D.J. Alexander, J. Nucl. Mater. 179–181 (1991) 733.
[14] R.L. Klueh, D.J. Alexander, in: A.S. Kumar, D.S. Gelles, R.K. Nanstad (Eds.), Effects of Radiation on Materials: 16th International Symposium, ASTM STP 1175, American Society for Testing and Materials, Philadelphia, 1994, p. 591.
[15] C. Wassilew, K. Ehrlich, J. Nucl. Mater. 191–194 (1992) 850.
[16] V.K. Shamardin, A.M. Pecherin, O.M. Vishkarev, V.P. Borisov, G.A. Tulyakov, in: Proceedings of the International Conference on Radiation and Material Science, Alushta, USSR, 1990, p. 3.
[17] D. Gilbon, J.-L. Seran, R. Cauvin, A. Fissolo, A. Alamo, F. LeNaour, V. Lévy, in: N.H. Packan, R.E. Stoller, A.S. Kumar (Eds.), Effects of Radiation on Materials: 14th International Symposium, ASTM STP 1046, vol. I, American Society for Testing and Materials, Philadelphia, 1990, p. 5.
[18] M.A. Sokolov, R.L. Klueh, G.R. Odette, K. Shiba, H. Tanigawa, in: M.L. Grossbeck, T.R. Allen, R.G. Lott, A.S. Kumar (Eds.), Effects of Radiation on Materials: 18th International Symposium, ASTM STP 1447, vol. 1, ASTM International, West Conshohocken, PA, 2004, p. 408.
[19] M.A. Sokolov, H. Tanigawa, G.R. Odette, K. Shiba, R.L. Klueh, J. Nucl. Mater. 367–370 (2007) 65.
[20] R.L. Klueh, D.J. Alexander, J. Nucl. Mater. 218 (1995) 151.
[21] D.S. Gelles, L.E. Thomas, in: J.W. Davis, D.J. Michel (Eds.), Ferritic Alloys for Use in Nuclear Energy Technologies, Metallurgical Society of AIME, Warrendale, PA, 1984, p. 559.
[22] J.M. Vitek, R.L. Klueh, Metall. Trans. A 14A (1983) 1047.
[23] R.W. Hertzberg, Deformation and Fracture Mechanics of Engineering Materials, 3rd Ed., Wiley, New York, 1989. p. 253.
[24] C.J. McMahon Jr., in: L.J. Bonis, J.J. Duga, J.J. Gilman (Eds.), Fundamental Phenomena in the Materials Sciences, vol. 4, Plenum, New York, 1967, p. 247.
[25] W.L. Hu, D.S. Gelles, in: F.A. Garner, C.H. Henager Jr., N. Igata (Eds.), Influence of Radiation on Material Properties: 14th International Symposium (Part II), ASTM STP 956, American Society for Testing and Materials, Philadelphia, 1987, p. 83.
[26] R.L. Klueh, J.M. Vitek, W.R. Corwin, D.J. Alexander, J. Nucl. Mater. 155–157 (1988) 973.
[27] R.L. Klueh, J.M. Vitek, J. Nucl. Mater. 161 (1989) 13.

[28] D.S. Gelles, W.L. Hu, F.H. Huang, G.D. Johnson, Alloy Development for Irradiation Performance, Semiannual Progress Report for Period Ending 30 September 1983, US Department of Energy, Office of Fusion Energy, DOE/ER-0045/11, March 1984, p. 115.
[29] W.L. Hu, D.S. Gelles, in: N.H. Packan, R.E. Stoller, A.S. Kumar (Eds.), Effects of Radiation on Materials: 14th International Symposium, ASTM STP 1046, vol. II, American Society for Testing and Materials, Philadelphia, 1989, p. 453.
[30] N. Saunders, X. Li, P. Miodownik, J.Ph. Schillé, in: J.-C. Zhao, M. Fahrmann, T. Pollock (Eds.), Proceedings of the Symposium on Material Design Approach and Experiences, The Materials Society, Warrendale, PA, 2001, p. 185.
[31] K. Anderko, L. Schäfer, E. Materna-Morris, J. Nucl. Mater. 179–181 (1991) 492.
[32] L. Schäfer, J. Nucl. Mater. 258–263 (1998) 1336.
[33] B.A. Chin, R.C. Wilcox, in: J.W. Davis, D.J. Michel (Eds.), Ferritic Alloys for Use in Nuclear Energy Technologies, Metallurgical Society of AIME, Warrendale, PA, 1984, p. 347.
[34] K. Shiba, in: Proceedings of the IEA Working Group Meeting on Ferritic/Martensitic Steels, 3–4 November 1997, Japan Atomic Energy Research Institute, Tokai, Japan, 1998, p. 119.
[35] K. Shiba, Y. Kohno, A. Kohyama, in: Report of IEA Workshop on Ferritic/Martensitic Steels, 2–3 November 2000, Japan Atomic Energy Research Institut, Tokai, Japan, 2001, p. 79.
[36] D.J. Alexander, P.J. Maziasz, C.R. Brinkman, in: P.K. Liaw, R. Viswanathan, K.L. Murty, E.P. Simonen, D. Frear (Eds.), Microstructure and Mechanical Properties of Aging Material, The Minerals, Metals and Materials Society, Warrendale, PA, 1993, p. 343.
[37] E.A. Little, L.P. Stoter, in: H.R. Brager, J.S. Perrin (Eds.), Effects of Irradiation on Materials: 11th Conference, ASTM STP 782, American Society for Testing and Materials, Philadelphia, 1982, p. 207.
[38] P.J. Maziasz, R.L. Klueh, in: N.H. Packan, R.E. Stoller, A.S. Kumar (Eds.), Effects of Irradiation on Materials: 14th International Symposium, ASTM STP 1046, vol. II, American Society for Testing and Materials, Philadelphia, 1990, p. 35.
[39] P.J. Maziasz, R.L. Klueh, in: R.E. Stoller, A.S. Kumar, D.S. Gelles (Eds.), Effects of Radiation on Materials: 15th International Symposium, ASTM STP 1125, American Society for Testing and Materials, Philadelphia, 1992, p. 1135.
[40] A. Kimura, H. Matsui, J. Nucl. Mater. 212–215 (1994) 701.
[41] Y. Kohno, A. Kohyama, M. Yoshino, K. Asakura, J. Nucl. Mater. 212–215 (1994) 707.
[42] A. Kimura, M. Narui, H. Kayano, J. Nucl. Mater. 191–194 (1992) 879.
[43] Y. Kohno, D.S. Gelles, A. Kohyama, M. Tamura, A. Hishinuma, J. Nucl. Mater. 191–194 (1992) 868.
[44] P.J. Grobner, Metall. Trans. 4 (1973) 251.
[45] H. Tanigawa, M.A. Sokolov, K. Shiba, R.L. Klueh, Fusion Sci. Technol. 44 (2003) 206.
[46] B. van der Schaaf, D.S. Gelles, S. Jitsukawa, A. Kimura, R.L. Klueh, A. Moeslang, G.R. Odette, J. Nucl. Mater. 283–287 (2000) 52.
[47] R.L. Klueh, P.J. Maziasz, J. Nucl. Mater. 187 (1992) 43.
[48] R.L. Klueh, D.J. Alexander, J. Nucl. Mater. 187 (1992) 60.
[49] R.L. Klueh, N. Hashimoto, M.A. Sokolov, P.J. Maziasz, J. Nucl. Mater. 357 (2006) 169.
[50] G.R. Odette, T. Yamamoto, H.J. Rathbun, M.Y. He, M.L. Hribernik, J.W. Rensman, J. Nucl. Mater. 323 (2003) 313.
[51] T. Yamamoto, G.R. Odette, H. Kishimoto, J.W. Rensman, P. Miao, J. Nucl. Mater. 356 (2006) 27.
[52] R.O. Ritchie, J.F. Knott, J.R. Rice, J. Mech. Phys. Solids 21 (1973) 395.